Electronic Supporting Information

Adsorption and dissolution of silver nanoparticles by iron oxide colloids under environmentally relevant conditions

Rui Wang,[a,b] Fei Dang,*[a] Cun Liu,[a] Deng-jun Wang,[c] Pei-xin Cui,[a] Hui-jun Yan,[a,b] and Dong-mei Zhou*[a]

a. Key Laboratory of Soil Environment and Pollution Remediation, Institute of Soil Science, Chinese Academy of Sciences, Nanjing 210008, China

b. University of Chinese Academy of Sciences, Beijing 100049, China

c. National Research Council Resident Research Associate at the United States Environmental Protection Agency, Ada, Oklahoma 74820, USA

* Corresponding Authors. Tel.: +86-25-86881180; Fax: +86-25-86881000.

E-mail Addresses: fdang@issas.ac.cn (F.D.); and dmzhou@issas.ac.cn (D.Z.).

Summary

SI includes 33 pages; 4 Tables; and 18 Figures.

Table of Contents

Figure S5. The volume-average hydrodynamic diameters（A and B) and number-average hydrodynamic diameters (C and D).

Figure S6. Sedimentation history of AgNPs (A), goethite (B), hematite (C), AgNPs-goethite (D), and AgNPs-hematite (E) over the time frame of 0 – 30 min under different experimental conditions.

Figure S7. Representative transmission electron microscopy (TEM) images, TEM-determined particle size distribution, TEM electron diffraction image, and dynamic light scattering (DLS) particle size distribution of AgNPs in stock suspension.

Figure S8. Zeta (ζ)-potentials of the AgNP, goethite, and hematite suspensions in 10 mM $NaNO_3$ as a function of pH.

Figure S9. Representative scanning electron microscopy images of goethite and hematite.

Figure S10. Calculated DLVO interaction energy between AgNPs and AgNPs, goethite and goethite, and hematite and hematite, based on $NaNO_3$ concentrations of 1, 10, and 100 mM, at pH 5.5 and pH 7.5, as a function of the separation distance using the Hamaker constant of A_{AgNPs} (6.99×10^{-20} J), $A_{goethite}$ (2.29×10^{-20} J) and $A_{hematite}$ (4.30×10^{-20} J).

Figure S11. Hydrodynamic diameter (D_h) of AgNPs (10 mg L^{-1}) as a function of pH and ionic strength (IS).

Figure S12. Hydrodynamic diameter (D_h) of goethite and hematite (100 mg L^{-1}) as a function of pH and IS.

Figure S13. Hydrodynamic diameter (D_h) of AgNPs-goethite and AgNPs-hematite as a function of pH and IS.

Figure S14. X-ray diffraction patterns of AgNPs-goethite and AgNPs-hematite at pH 5.5 and pH 7.5 in 100 mM $NaNO_3$.

Figure S15. Attenuated total reflectance-Fourier transform infrared spectroscopy spectra of the interaction of AgNPs with goethite and hematite.

Figure S16. Ag k-space EXAFS spectra (A) and the Fourier transforms (B) for Ag foil and goethite after batch experiments.

Figure S17. Cumulative pore volume calculated from BET-N_2 method.

Figure S18. Adsorption isotherms of Ag^+ on goethite and hematite in 10 mM $NaNO_3$ at pH 5.5 and pH 7.5.

Text S1. Hydrodynamic diameters (D_h) and zeta (ζ)-potentials of AgNPs and iron oxides.

The hydrodynamic diameters (D_h) and ζ-potentials of the AgNPs and iron oxides were monitored using dynamic light scattering (DLS; BI-200SM, Brookhaven, USA) and a zeta-potential analyzer (Zetasizer Nanosizer ZS, Malvern Instrument Co., UK), respectively.

For DLS analysis, the samples were mixed vigorously for 3 s using a vortex mixer (SCILOGEX MX-S, USA) and then quickly used in the measurements. Each autocorrelation function was accumulated over 30 s, and the intensity-weighted hydrodynamic diameter was derived using second-order cumulant analysis (Brookhaven software). For the ζ-potential analysis, the solids were collected after completion of the batch experiments, centrifuged at 3000×*g* for 10 min, rinsed with Milli-Q water twice, and freeze-dried. They were then re-suspended using the desired electrolytes and their ζ-potentials were characterized. Triplicate experiments were performed for DLS and ζ-potential measurements.

The initial aggregation rate was calculated using a linear least-squares analysis of the increase in D_h with time. As shown in Figure 4 in the main text, the intensity of the scattered light from the binary AgNP-goethite suspension was significantly greater than that from the AgNPs but closer to that of goethite, indicating that goethite was the dominant light scatterer in the binary suspensions. Therefore, for the binary systems, the analysis was performed during the period of time that D_h increased until it was 1.3-fold higher than the initial D_h of the iron oxides. In the case of the slow homoaggregation of goethite, in which D_h failed to increase within the short time by 1.3-fold, a linear aggregation was performed over a longer time (> 20 min). This approach to determining the heteroaggregation rate was similar to that used by Huynh et al..[1]

Text S2. Derjaguin-Landau-Verwey-Overbeek (DLVO) interaction energy calculation.

In this study, classical DLVO theory, which takes into account both van der Waals (vdW) and electrostatic double-layer (EDL) interactions, was applied to quantitatively describe the stability of the AgNPs, goethite, and hematite under solution chemistries similar to those of the batch experiments. The vdW and EDL interaction energies were calculated for the AgNP-AgNP, goethite-goethite, and hematite-hematite systems, assuming a sphere-sphere configuration, and for the AgNP-goethite and AgNP-hematite systems, assuming a sphere-plate configuration. The expressions for calculating the vdW interaction energy (Φ_{vdW}) for the sphere-sphere and sphere-plate configurations are presented in Eqs. (1) and (2), respectively,[2-4]

$$\Phi_{vdW} = -\frac{A_{131} r_{h1} r_{h2}}{6h(r_{h1}+r_{h2})}\left[1+\frac{14h}{\lambda}\right]^{-1} \qquad (1)$$

$$\Phi_{vdW} = -\frac{A_{132} r_h}{6h}\left[1+\frac{14h}{\lambda}\right]^{-1} \qquad (2)$$

where r_{h1} and r_{h2} in Eq. (1) refer to the average hydrodynamic radii of the two interacting particles (AgNPs, goethite, or hematite) determined by DLS measurements (see Table S1); r_h in Eq. (2) refers to the average hydrodynamic radius of AgNPs; h is the separation distance between two particles; λ is the characteristic wavelength of the interaction (usually 100 nm)[2]; and A_{131} and A_{132} are the Hamaker constants for AgNPs-water-AgNPs (or goethite-water-goethite, or hematite-water-hematite) and AgNPs-water-goethite (or AgNPs-water-hematite), respectively, obtained from the Hamaker constants of the individual materials using Eqs. (3) and (4):[5]

$$A_{131} = (\sqrt{A_1} - \sqrt{A_{water}})(\sqrt{A_1} - \sqrt{A_{water}}) \qquad (3)$$

$$A_{132} = (\sqrt{A_{AgNPs}} - \sqrt{A_{water}})(\sqrt{A_2} - \sqrt{A_{water}}) \quad (4)$$

where A_1 is the Hamaker constant of the AgNPs ($A_{AgNPs} = 6.99\times10^{-20}$ J),[6] of goethite ($A_{goethite} = 2.29\times10^{-20}$ J),[7] or of hematite ($A_{hematite} = 4.30\times10^{-20}$ J)[8]; A_2 is $A_{goethite}$ or $A_{hematite}$; and A_{water} is the Hamaker constant of water (3.7×10^{-20} J).[9]

The EDL interaction energy (Φ_{EDL}) for the sphere-sphere and sphere-plate configurations can be calculated using Eqs. (5) (6), respectively.[3, 4, 10]

$$\Phi_{EDL} = 0.5\pi\varepsilon_0\varepsilon_r \frac{r_{h1}r_{h2}}{(r_{h1}+r_{h2})}\{2\Psi_1\Psi_2 \ln\left[\frac{1+\exp(-\kappa h)}{1-\exp(-\kappa h)}\right] + ({\Psi_1}^2 + {\Psi_2}^2)\ln[1 - \exp(-2\kappa h)]\} \quad (5)$$

$$\Phi_{EDL} = 0.5\pi\varepsilon_0\varepsilon_r r_h\{2\Psi_1\Psi_2 \ln\left[\frac{1+\exp(-\kappa h)}{1-\exp(-\kappa h)}\right] + ({\Psi_1}^2 + {\Psi_2}^2)\ln[1 - \exp(-2\kappa h)]\} \quad (6)$$

$$\kappa = \sqrt{\frac{1000e^2\sum n_{j0}{z_j}^2}{\varepsilon_0\varepsilon_r kT}} \quad (7)$$

where ε_0 and ε_r are the dielectric permittivity of the vacuum (8.854×10^{-12} C/Vm) and water (78.5 at 298 K), respectively; ψ_1 and ψ_2 are the ζ-potentials of AgNPs, goethite, and hematite in Eq. (5); ψ_1 and ψ_2 are the ζ-potentials of AgNPs and goethite/hematite, respectively, in Eq. (6) (see Table S1); κ is the Debye-Hückel parameter, which is determined using Eq. (7)[4]; e is the electron charge (1.602×10^{-19} C); n_{j0} is the number concentration of the ion in the bulk suspension (6.022×10^{23} mol^{-1}); z_j is the ion valence (note the valence for monovalent $NaNO_3$); k is the Boltzmann constant (1.38×10^{-23} J/K); and T is the absolute temperature (298 K).

DLVO theory as described above is based on a series of assumptions, including that the surfaces are molecularly smooth and spherically shaped for both the colloids and the collectors. In this study, however, neither goethite nor hematite was spherical

(Figure S6). The particle size was obtained via DLS measurements, which was also calculated based on the assumption of spherically shaped goethite and hematite. Nonetheless, the above DLVO calculation provides a first approximation of the anticipated changes in the mean interaction energy in response to the variability in the electrolyte concentration and solution pH.

Text S3. Langmuir modeling.

The Langmuir model was used to describe the adsorption of AgNPs by goethite and hematite based on the hypothesis that only one type of surface site exists for AgNPs:

$$\Gamma_e = \frac{\Gamma_{max} K_L C_e}{1 + K_L C_e} \quad (8)$$

where Γ_e (mg m^{-2}) is the surface coverage of goethite and hematite by AgNPs; Γ_{max} (mg m^{-2}) is the maximum surface coverage of goethite and hematite by AgNPs; K_L (L mg^{-1}) is the constant related to the free energy of adsorption; and C_e (mg L^{-1}) represents the equilibrium concentrations of total Ag in the suspensions. The adsorption data were well fitted by the Langmuir model. The model-fitted parameters are listed in Table S2.

Table S1. Average hydrodynamic diameter (D_h) and zeta (ζ)-potentials of the silver nanoparticles (AgNPs), goethite, and hematite used in the Derjaguin-Landau-Verwey-Overbeek (DLVO) calculations based on the different experimental conditions. The data are expressed as the mean ± SD (n = 3).

pH	**$NaNO_3$**	**D_h (nm)**			**ζ-potential (mV)**		
	(mM)	**AgNPs**	**Goethite**	**Hematite**	**AgNPs**	**Goethite**	**Hematite**
5.5	1	77.7±1.7	278±5	421±39	–31.9±2.8	43.6±0.4	24.8±0.6
5.5	10	82.7±3.0	452±14	871±85	–29.7±1.2	35.2±1.0	16.3±2.1
5.5	100	92.1±7.2	505±14	937±14	–23.3±1.4	28.0±1.6	16.0±1.0
7.5	1	79.6±0.8	513±10	913±98	–36.8±0.7	23.8±1.1	–6.0±0.5
7.5	10	78.3±2.5	608±3	915±135	–32.8±1.3	14.6±1.3	–4.1±0.2
7.5	100	82.9±12.0	609±8	947±107	–26.0±1.6	13.1±0.7	–3.5±0.1

Table S2. Langmuir model-fitted parameters for AgNP adsorption by goethite and hematite.

		Goethite			Hematite		
pH	**$NaNO_3$ (mM)**	**Γ_{max} [a] (mg m^{-2})**	**R**	**K_L [b] (L mg^{-1})**	**Γ_{max} [a] (mg m^{-2})**	**R**	**K_L (L mg^{-1})**
5.5	1	0.095	0.97	6.62	0.016	0.87	0.28
5.5	10	0.187	0.99	2.41	0.017	0.98	0.66
5.5	100	0.326	0.97	2.52	0.020	0.98	0.76
7.5	1	0.072	0.98	6.15	0.014	0.97	0.96
7.5	10	0.114	0.99	2.34	0.014	0.96	1.59
7.5	100	0.215	0.98	0.60	0.022	0.97	0.27

[a] Γ_{max} is the maximum surface coverage of goethite and hematite by AgNPs (mg m^{-2}).

[b] K_L is the constant related to the free energy of adsorption (L mg^{-1}).

Table S3. Calculated DLVO interaction energies based on the different experimental conditions.

		AgNPs-AgNPs			**Goethite-goethite**			**Hematite-hematite**			**AgNPs-goethite**			**AgNPs-hematite**		
pH	**$NaNO_3$**	**Φ_{max}[a]**	**Φ_{min2}[a]**	**h[b]**	**Φ_{max}**	**Φ_{min2}**	**h**	**Φ_{max}**	**Φ_{min2}**	**h**	**Φ_{max}**	**Φ_{min2}**	**h**	**Φ_{max}**	**Φ_{min2}**	**h**
	(mM)	**(kT)**	**(kT)**	**(nm)**	**(kT)**	**(kT)**	**(nm)**	**(kT)**	**(kT)**	**(nm)**	**(kT)**	**(kT)**	**(nm)**	**(kT)**	**(kT)**	**(nm)**
5.5	1	47.4	-0.004	112	355.6	-0.003	134	180.2	-0.001	145	< 0	NA[c]	NA	< 0	NA	NA
5.5	10	34.5	-0.057	26	338.2	-0.072	32	145.6	-0.017	34	< 0	NA	NA	< 0	NA	NA
5.5	100	8.3	-0.847	5	176.1	-0.951	7	131.2	-0.190	8	< 0	NA	NA	< 0	NA	NA
7.5	1	66.4	-0.004	116	183.2	-0.007	119	19.1	-0.002	109	< 0	NA	NA	5.9	-0.002	113
7.5	10	41.7	-0.051	27	56.1	-0.147	25	5.5	-0.035	22	< 0	NA	NA	2.3	-0.024	24
7.5	100	12.2	-0.698	5	16.8	-1.832	5	0.1	-0.506	4	< 0	NA	NA	0.1	-0.348	4

[a] Φ_{max} and Φ_{min2} are maximum repulsive energy barrier and attractive secondary minimum, respectively; k is the Boltzmann constant (1.38×10^{-23} J/K), and T is the absolute temperature (298 K).

[b] h is the separation distance from the AgNP (or goethite, or hematite) surface to the secondary minimum.

[c] NA denotes not applicable.

Table S4. EXAFS fitting parameters at the Ag K-edge for various samples (S_0^2=0.854).

Sample	**Shell**	N^a	R(Å)^b	σ^2(Å^2)^c	ΔE_0(eV)^d	**R factor**
Ag foil	Ag-Ag	12	2.86	0.0097	1.5	0.0013
pH 5.5	Ag-Ag	5.8	2.84	0.0029	-0.8	0.0024
pH 7.5	Ag-Ag	4.7	2.86	0.0028	-0.3	0.0144

$^a N$ is coordination number; $^b R$ is bond distance; $^c\sigma^2$ is Debye-Waller factor; ^{d} ΔE_0 is the inner potential correction. R-factor indicates the goodness of the fit. Amplitude reduction factor S_0^2 was set to 0.830, according to the Ag foil fit by fixing coordination number as the known crystallographic value.

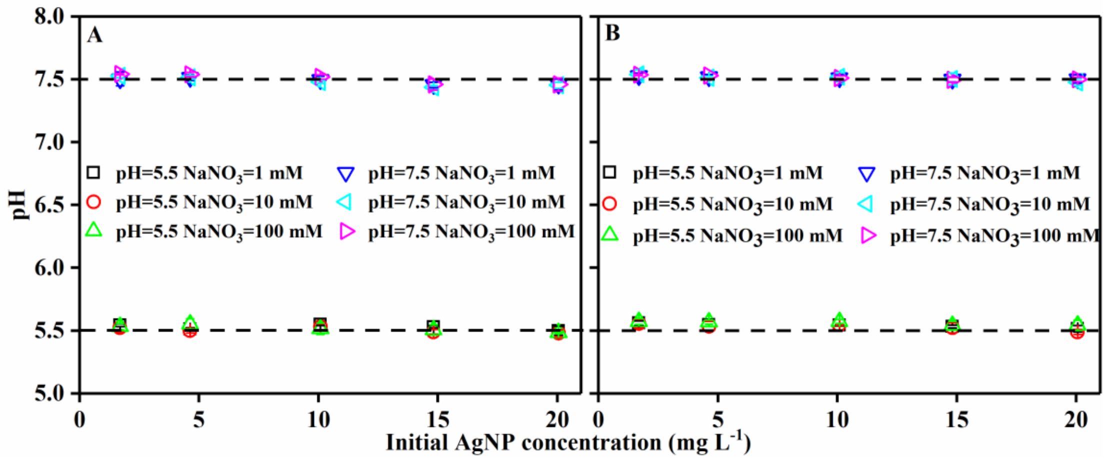

Figure S1. Variation in the suspension pH used to measure silver nanoparticle (AgNP) adsorption by goethite (A) and hematite (B), respectively. The data are expressed as the mean ± SD (n = 3). The suspension pH was maintained at 5.5 and 7.5 using 10 mM 2-(N-morpholino)ethanesulfonic acid (MES, Biosharp Corp., China) and 3-morpholinopropanesulfonic acid (MOPS, Biosharp Corp.), respectively. The concentration of goethite and hematite in the respective suspensions was 2,500 mg L^{-1}.

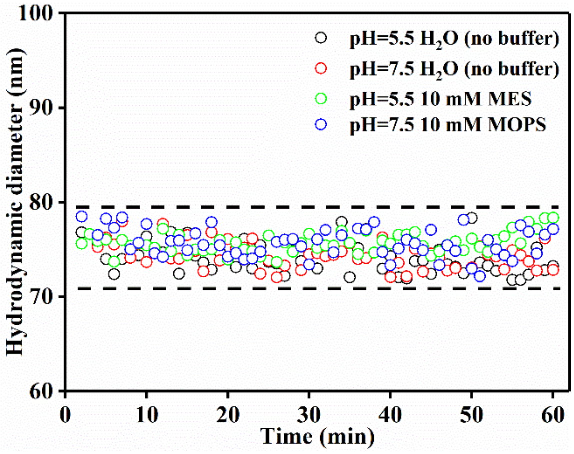

Figure S2. Average hydrodynamic diameter (D_h) of AgNPs at pH 5.5 and pH 7.5 with 10 mM MES (pH 5.5) or 10 mM MOPS (7.5) or without buffer.

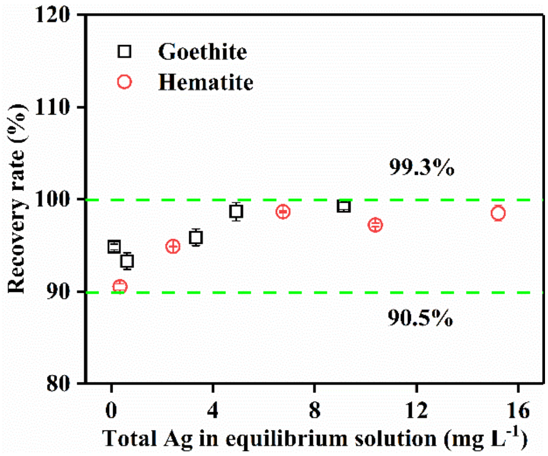

Figure S3. Mass recoveries of Ag during the filtering process in 100 mM $NaNO_3$ at pH 7.5. The mass recoveries of 90.5–99.3% suggested negligible Ag loss due to blocking of goethite or hematite during filtering process. The data are expressed as the mean ± SD (n = 3)

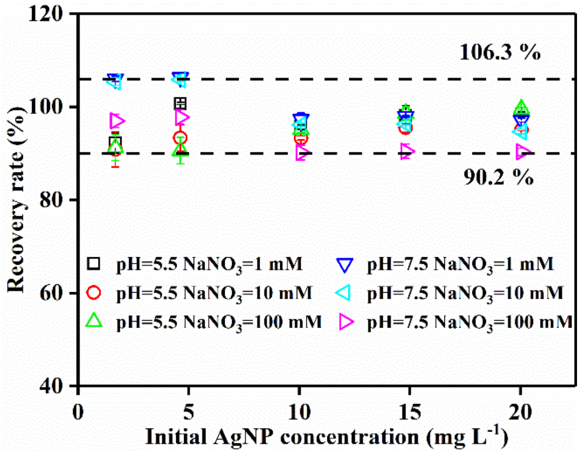

Figure S4. Mass recoveries of Ag during the 24-h adsorption experiment in the absence of goethite and hematite. The mass recoveries of 90.2–106.3% suggested negligible Ag loss due to adsorption onto the vials and filtering membranes. The data are expressed as the mean ± SD (n = 3).

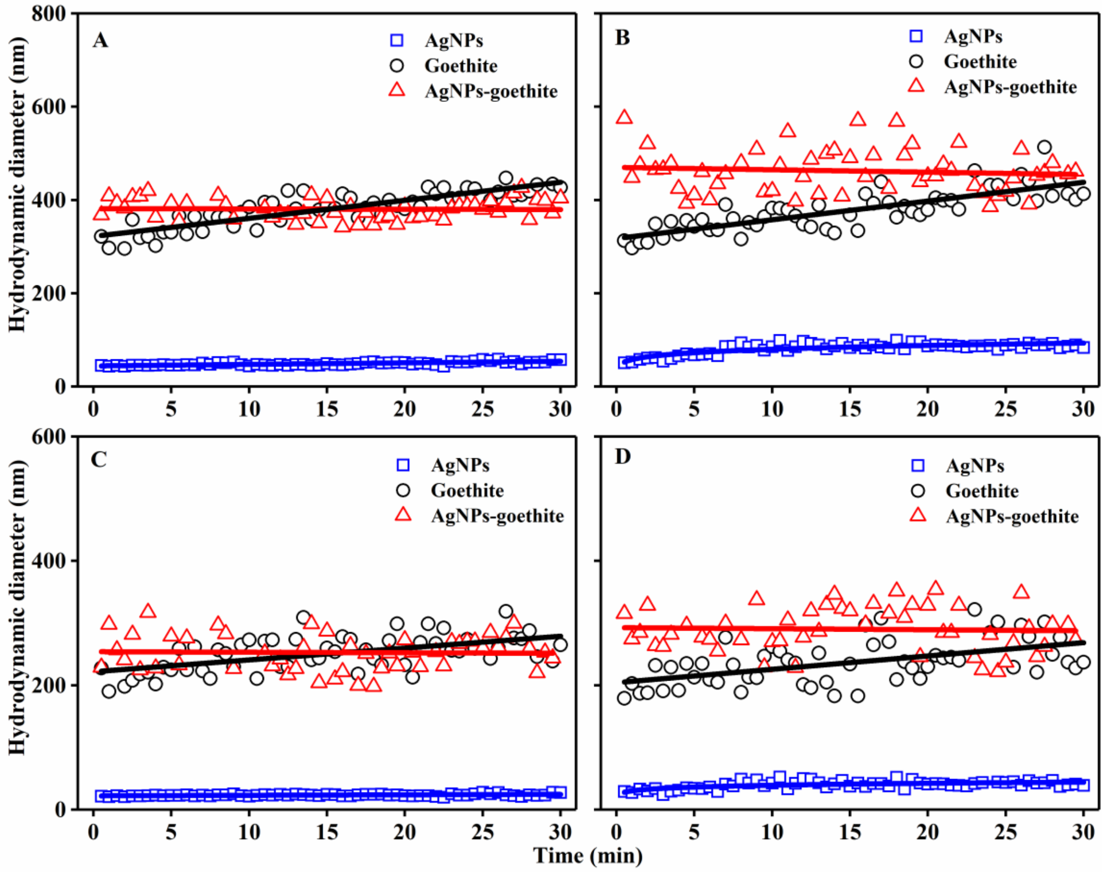

Figure S5 The volume-average hydrodynamic diameters（A and B) and number-average hydrodynamic diameters (C and D). Homoaggregation profiles of AgNPs at 10 mg L^{-1} and goethite at 100 mg L^{-1}, as well as heteroaggregation profiles of AgNPs at 1 mg L^{-1} and goethite at 100 mg L^{-1}. All experiments were conducted at 10 mM (A and C) and 100 mM (B and D) $NaNO_3$ at pH 5.5.

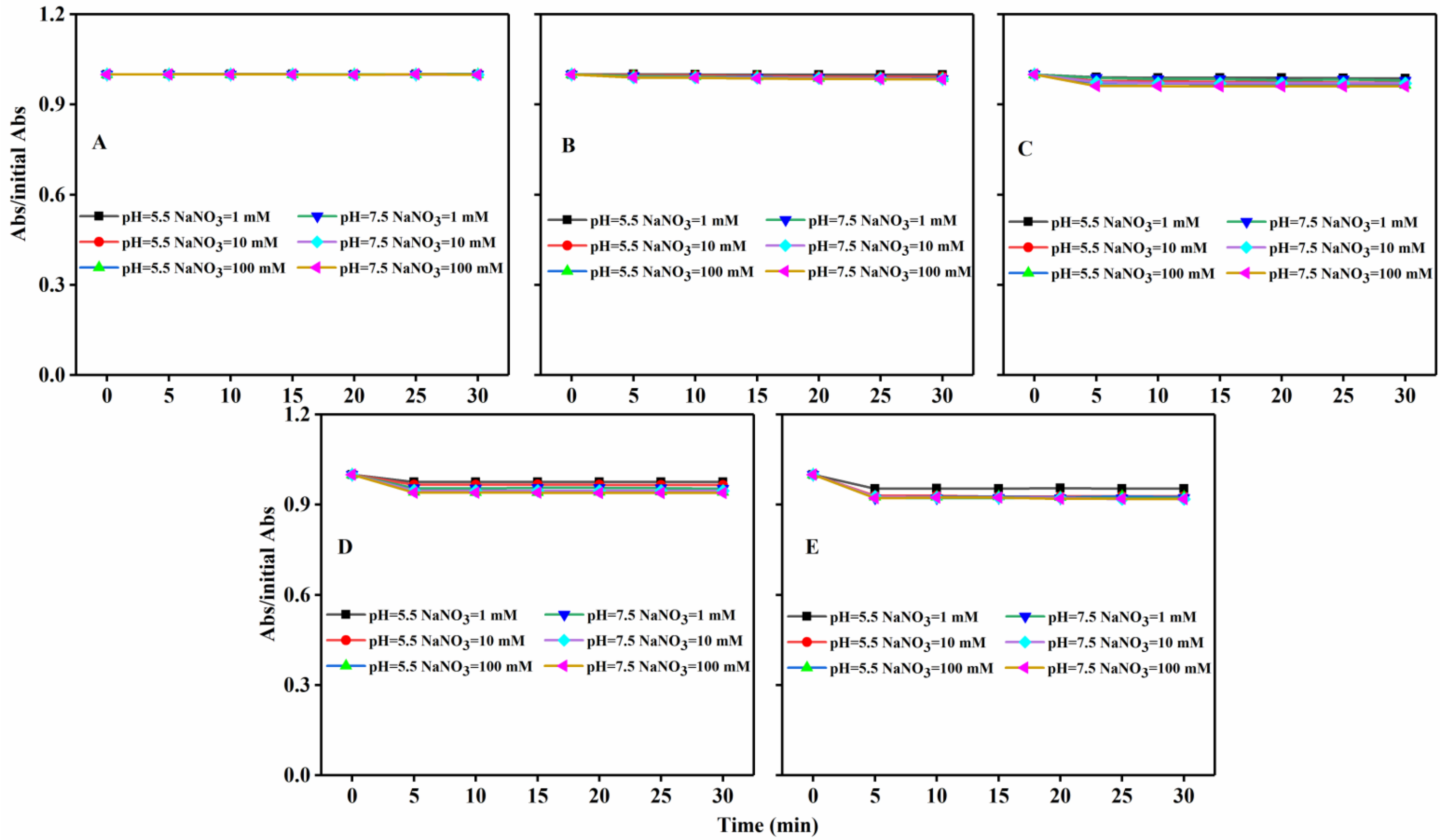

Figure S6 Sedimentation history of AgNPs (A), goethite (B), hematite (C), AgNPs-goethite (D), and AgNPs-hematite (E) over the time frame of 0 – 30 min under different experimental conditions. Sedimentation was monitored by measuring optical density at 406 nm (AgNPs, AgNPs-goethite and AgNPs-hematite), at 425 nm (goethite and hematite) using UV–vis spectrophotometer.

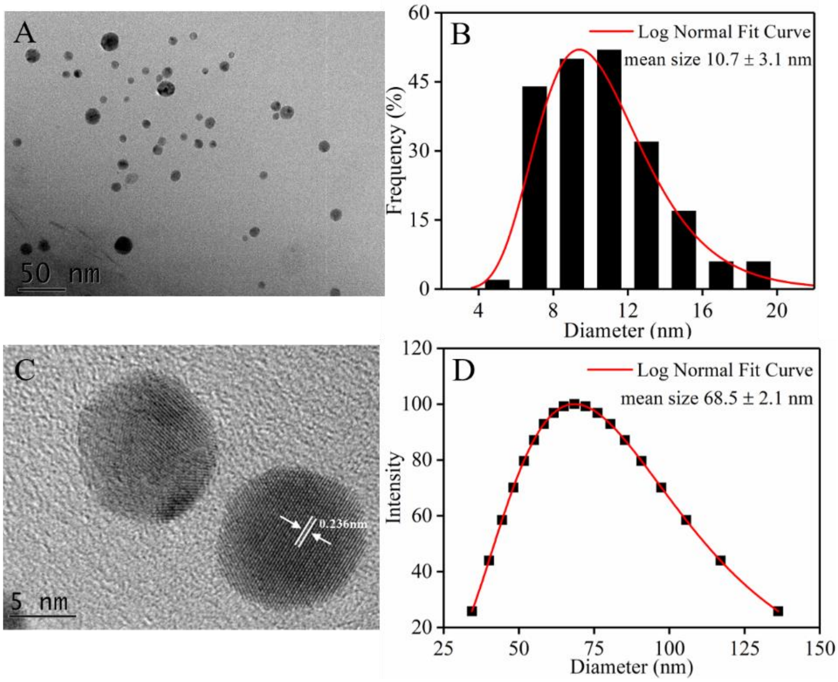

Figure S7. Representative transmission electron microscopy (TEM) image (A), TEM-determined particle size distribution (B), TEM electron diffraction image (C), and dynamic light scattering (DLS) particle size distribution (D) of AgNPs in stock suspension. Scale bar = 50 nm in (A) and 5 nm in (C).

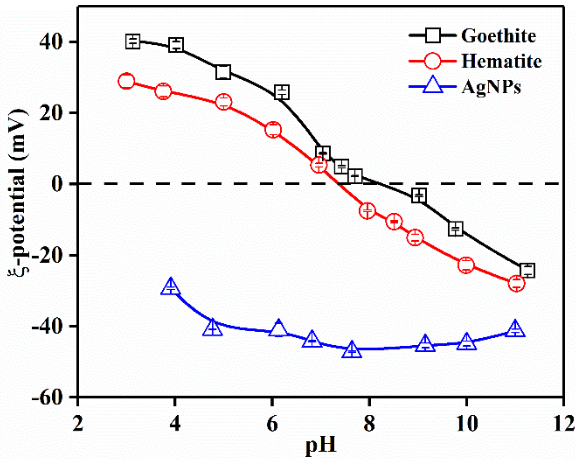

Figure S8. Zeta (ζ)-potentials of the AgNP, goethite, and hematite suspensions in10 mM $NaNO_3$ as a function of pH. The pH was adjusted using 1 mM HNO_3 or NaOH. The AgNPs were negatively charged under the tested pH (4.0–11.0) conditions. Both goethite and hematite became more negatively charged at higher pH, due to the enhanced deprotonation effect. At a specified pH, goethite was more positively charged than hematite. The isoelectric point (IEP) was 8.2 for goethite and 7.4 for hematite. The data are expressed as the mean ± SD (n = 6).

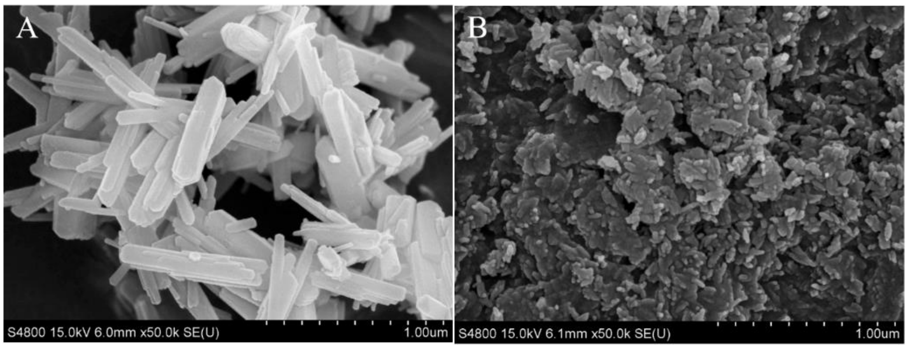

Figure S9. Representative scanning microscopy images of goethite (A) and hematite (B). Scale bar = 1 μm.

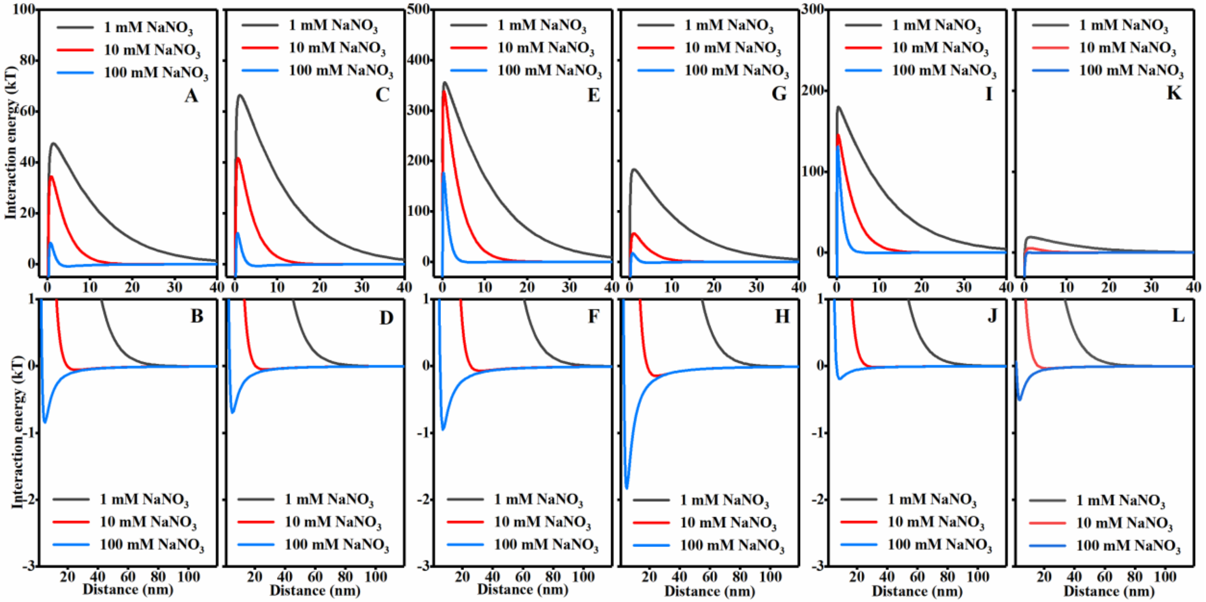

Figure S10. Calculated DLVO interaction energy profiles between AgNPs and AgNPs (A–D), goethite and goethite (E–H), and hematite and hematite (I–L) based on $NaNO_3$ concentrations of 1, 10, and 100 mM, at pH 5.5 (A, B, E, F, I, and J) and pH 7.5 (C, D, G, H, K, and L), as a function of the separation distance using the Hamaker constant of A_{AgNPs} (6.99×10^{-20} J), $A_{goethite}$ (2.29×10^{-20} J), and $A_{hematite}$ (4.30×10^{-20} J). Panels A, C, E, J, I, and K shows the maximum repulsive energy barrier (Φ_{max}), and panels B, D, F, H, J, and L the secondary minimum (Φ_{min2}) of the interaction energy profile.

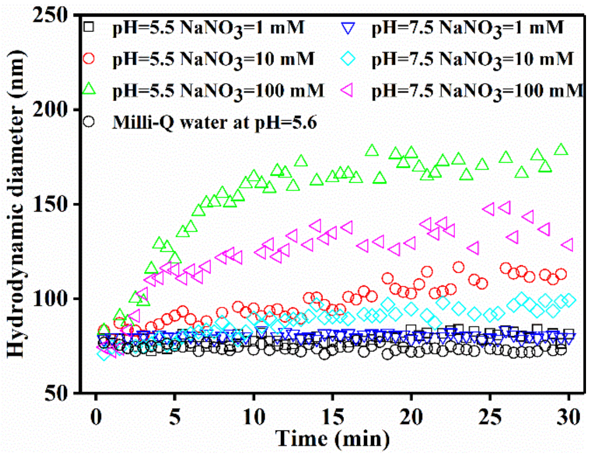

Figure S11. Hydrodynamic diameter (D_h) of AgNPs (10 mg L^{-1}) as a function of pH and ionic strength (IS).

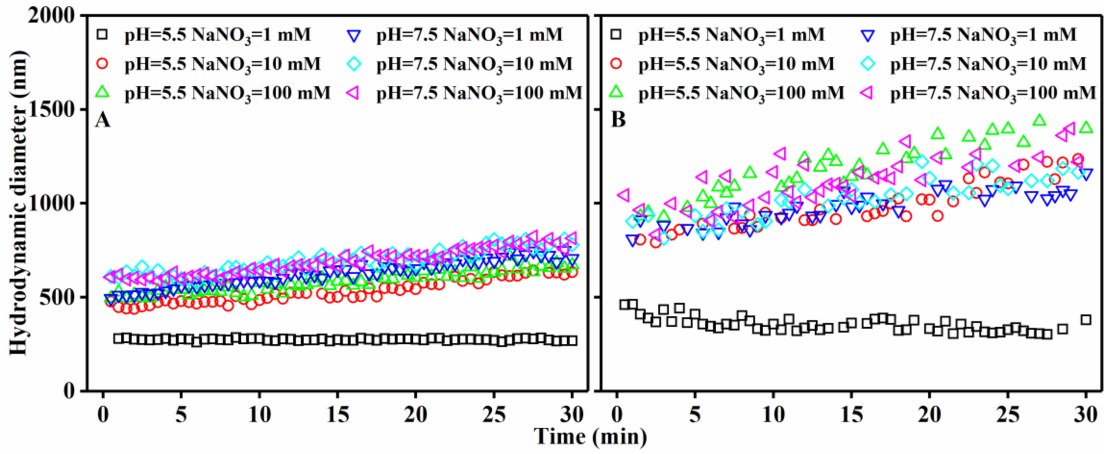

Figure S12. Hydrodynamic diameter (D_h) of goethite (A) and hematite (100 mg L^{-1}) (B) as a function of pH and IS.

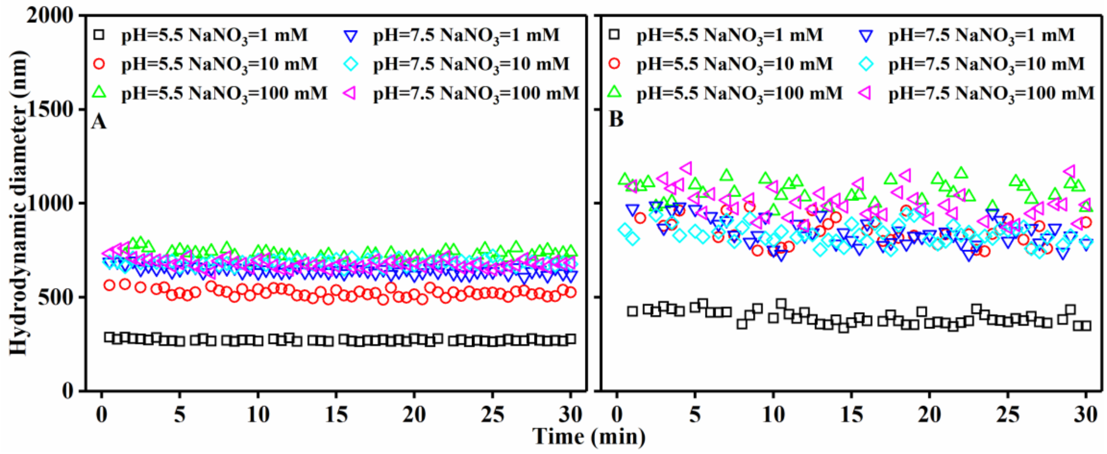

Figure S13. Hydrodynamic diameter (D_h) of AgNPs-goethite (A) and AgNPs-hematite (B) as a function of pH and IS. AgNPs: 1 mg L^{-1}; iron oxides: 100 mg L^{-1}.

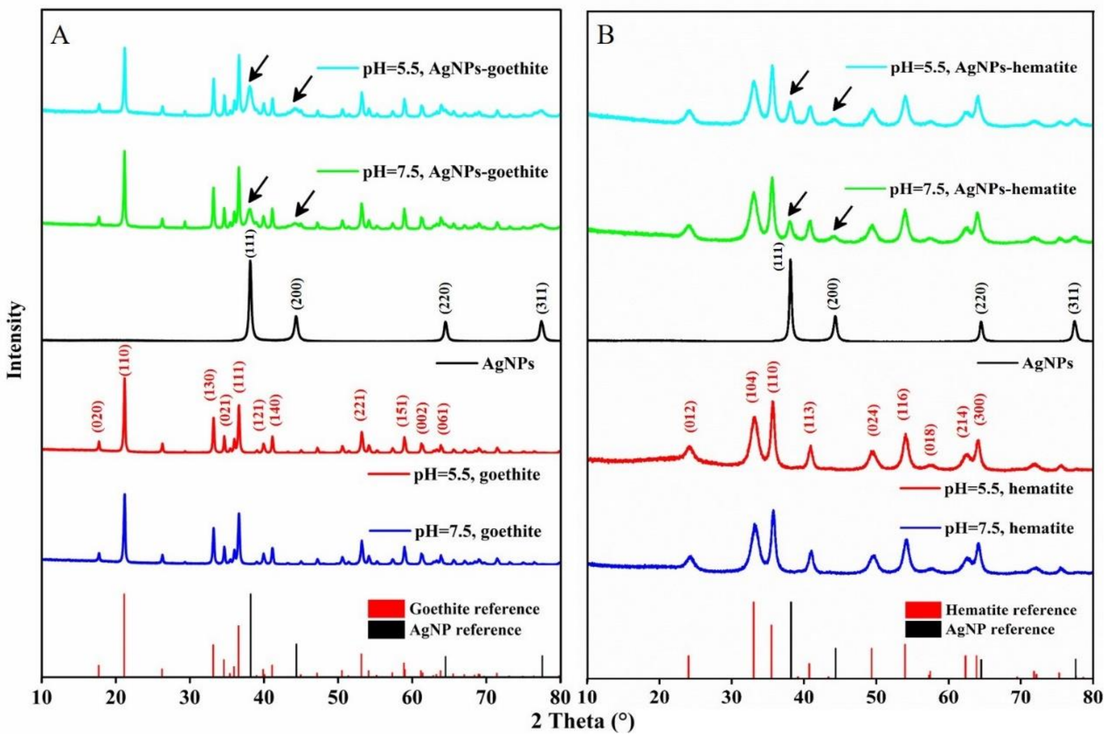

Figure S14. X-ray diffraction patterns of AgNPs-goethite (A) and AgNPs-hematite (B) at pH 5.5 and pH 7.5 in 100 mM $NaNO_3$. To better detect the silver signal, the initial concentration of AgNPs was 99.7 mg L^{-1} and the concentration of iron oxides 2,500 mg L^{-1}.

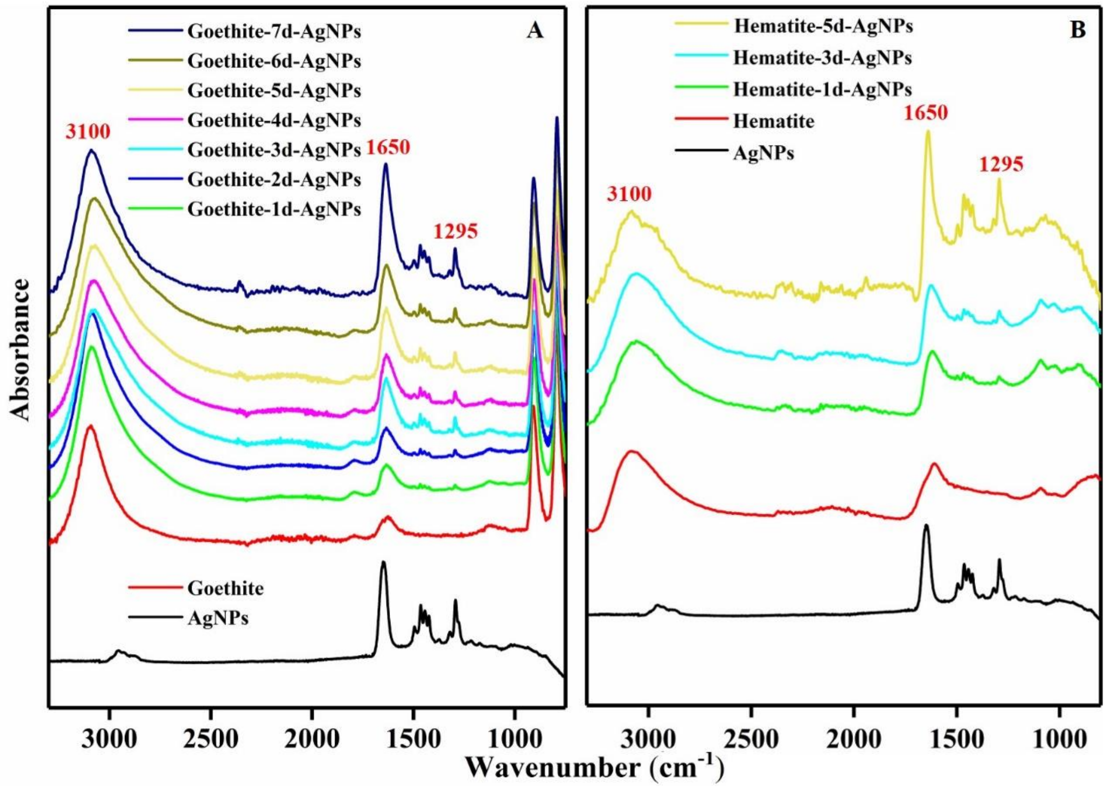

Figure S15. Attenuated total reflectance-Fourier transform infrared spectroscopy spectra of the interaction of the AgNPs with goethite (A) and hematite (B). 1d–7d represent the 1–7 drops of AgNPs (99.7 mg L^{-1}, approximately 10 µL per drop) added to the goethite or hematite.

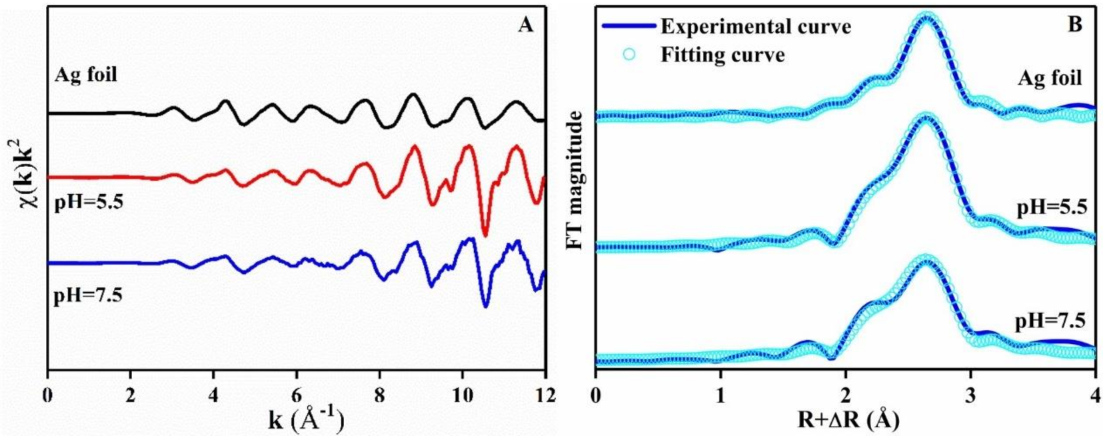

Figure S16. Ag k-space EXAFS spectra (A) and the Fourier transforms (B) for Ag foil and goethite after batch experiments.

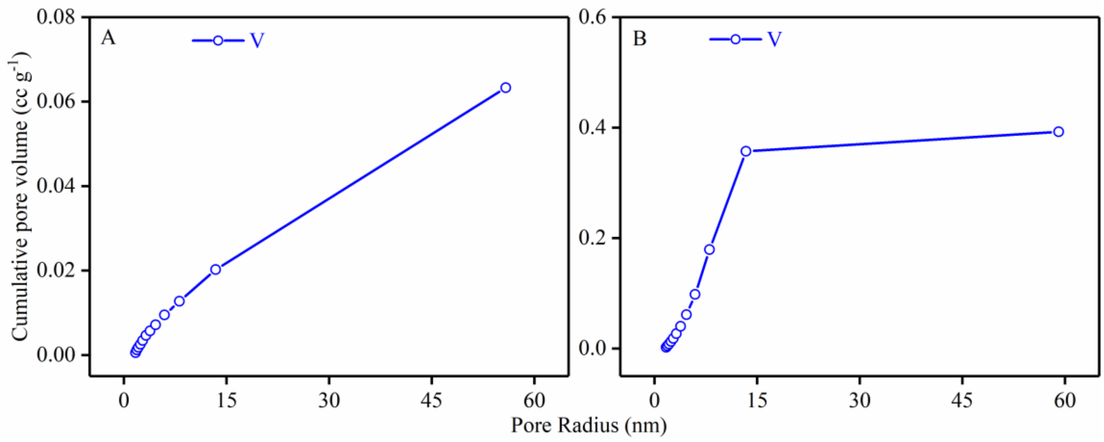

Figure S17 Cumulative pore volume calculated from BET-N_2 method.

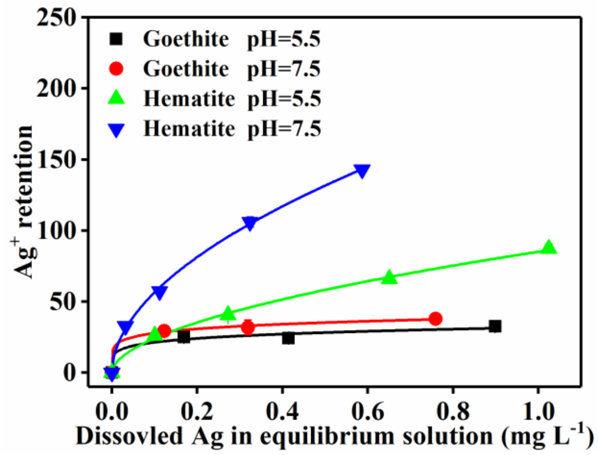

Figure S18. Adsorption isotherm of Ag$^+$ ion on goethite and hematite in 10 mM $NaNO_3$ at pH 5.5 and pH 7.5. The data are expressed as the mean ± SD (n = 3).

References:

1. H. Khanh An, J. M. McCaffery and K. L. Chen, Heteroaggregation of multiwalled carbon nanotubes and hematite nanoparticles: rates and mechanisms, *Environmental Science & Technology*, 2012, **46**, 5912-5920.
2. J. Gregory, Approximate expressions for retarded vanderwaals interaction, *Journal of Colloid and Interface Science*, 1981, **83**, 138-145.
3. M. Elimelech, J. Gregory, X. Jia and R. Williams, Particle deposition and aggregation measurement, modeling and simulation. Butterworth-Heinemann, Woburn, MA, 1995.
4. M. Tong, H. Ma and W. P. Johnson, Funneling of flow into grain-to-grain contacts drives colloid-colloid aggregation in the presence of an energy barrier, *Environmental Science & Technology*, 2008, **42**, 2826-2832.
5. J. Bergendahl and D. Grasso, Prediction of colloid detachment in a model porous media: Thermodynamics, *AIChE Journal*, 1999, **45**, 475-484.
6. A. M. El Badawy, K. G. Scheckel, M. Suidan and T. Tolaymat, The impact of stabilization mechanism on the aggregation kinetics of silver nanoparticles, *Science of the total environment*, 2012, **429**, 325-331.
7. C. Xu, K. Deng, J. Li and R. Xu, Impact of environmental conditions on aggregation kinetics of hematite and goethite nanoparticles, *Journal of Nanoparticle Research*, 2015, **17**, 1-13.
8. M. Schudel, S. H. Behrens, H. Holthoff, R. Kretzschmar and M. Borkovec, Absolute aggregation rate constants of hematite particles in aqueous suspensions: A comparison of two different surface morphologies, *Journal of Colloid and Interface Science*, 1997, **196**, 241-253.
9. D. Wang, C. M. Park, A. Masud, N. Aich and C. Su, Carboxymethylcellulose Mediates the Transport of Carbon Nanotube–Magnetite Nanohybrid Aggregates in Water-Saturated Porous Media, *Environmental Science & Technology*, 2017, **51**, 12405-12415.
10. R. Hogg, T. W. Healy and D. W. Fuerstenau, Mutual coagulation of colloidal dispersions, *Transactions of the Faraday Society*, 1966, **62**, 1638-1651.